Quantitative CT assessment of lung injury after successful cardiopulmonary resuscitation in a porcine cardiac arrest model of different downtimes

Zhifeng Liu[1#], Qingyu Liu[1,2#], Gongfa Wu[1#], Haigang Li[1,2], Yue Wang[2], Rui Chen[2], Cai Wen[2], Qin Ling[1], Zhengfei Yang[1,2,3], Wanchun Tang[1,2,3]

[1]Zengcheng District People's Hospital of Guangzhou, Guangzhou 511300, China; [2]Sun Yat-sen Memorial Hospital, Sun Yat-sen University, Guangzhou 510120, China; [3]Weil Institute of Emergency and Critical Care Research, School of Medicine, Virginia Commonwealth University, Richmond, VA, USA

[#]These authors contributed equally to this work.

Correspondence to: Zhengfei Yang, MD, PhD; Wanchun Tang, MD. Sun Yat-sen Memorial Hospital, Sun Yat-sen University, 107 Yan Jiang Xi Road, Guangzhou 510120, China. Email: yangzhengfei@vip.163.com; wanchun.tang@vcuhealth.org.

Background: Utilize quantitative computed tomography (QCT) to detect and evaluate the severity of lung injury after successful cardiopulmonary resuscitation (CPR) in a porcine cardiac arrest (CA) model with different downtimes.

Methods: Twenty-one male domestic pigs weighing 38±3 kg were randomized into 3 groups: the sham group (n=5), the ventricular fibrillation (VF) 5 min (VF5) group (n=8), and the VF 10 min (VF10) group (n=8). VF was induced and untreated for 5 (VF5 group) or 10 (VF10 group) min before the commencement of manual CPR. Eight animals (8/8, 100%) in VF5 and 6 (6/8, 75%) in VF10 were successfully resuscitated. Chest QCT scans and arterial blood gas tests were performed at baseline and 6 h post-resuscitation. The QCT score, volume, and weight of ground-glass opacification (GGO), which was defined as poorly aerated regions with a CT value ranging from −500 Hounsfield units (HU) to −100 HU, and intense parenchymal opacification (IPO), which was defined as a non-aerated area with a CT value greater than −100 HU, were quantitatively measured.

Results: Significantly shorter durations of CPR and fewer defibrillations were observed in the VF5 group compared with the VF10 group [duration of CPR: VF5 (6±0 minutes) versus VF10 (8.3±1.5 minutes), $P<0.05$; numbers of defibrillation: VF5 (1±0) versus VF10 (2.2±0.8), $P<0.05$]. Compared with the baseline or sham animals, declining gas exchanges (end-tidal CO_2, PO_2, oxygen index) were observed in both VF groups; however, there were no significant differences in gas exchanges between the VF groups. Compared with the VF5 group, the GGO QCT score, volume, and weight were significantly greater in the VF10 group ($P=0.002$, 0.001, and 0.002 respectively), while no significant differences were found in the IPO QCT score, volume, or weight between two the VF groups ($P=0.354$, 0.447, and 0.512 respectively).

Conclusions: QCT analysis enables unique non-invasive assessments of different lung injuries (IPO and GGO lesions) that can clearly distinguish heterogeneous lesions and allow for early detection and quantitative monitoring of the severity of lung injury following CPR. QCT could provide a basis for clinical early ventilation strategy management after CPR.

Keywords: Lung injury; cardiac arrest (CA); cardiopulmonary resuscitation (CPR); computed tomography (CT)

Introduction

Increasing numbers of patients suffering from cardiac arrest (CA) have achieved successful restoration of spontaneous circulation (ROSC) after early and effective cardiopulmonary resuscitation (CPR) (1,2). However, many studies have also shown that the total morbidity of lung injuries after CPR remains high, ranging from 21–97% (3,4).

The American Heart Association (AHA) guidelines increased the compression depth requirement of CPR to at least 50 mm after 2010 (5,6). Accompanying the need to exert physical force on the victim's chest is the risk of lung injury (7). Lung injury is frequently observed related to CPR, with pathological characteristics such as pulmonary hemorrhage, pulmonary edema, and atelectasis (8,9). Improper mechanical ventilation may convert the mechanical injury to biotrauma, activating the intracellular signal pathways and exacerbating local inflammation caused by inflammatory mediators in the lung (10). Moreover, as the active substances in metabolites pass through or remain in the lung, the damage of respiratory membrane function is aggravated. Furthermore, during the inflammatory cascade generated by lung ischemia-reperfusion, the inflammatory cells infiltration and a large amount of red blood and inflammatory cell exudate exacerbates lung injury (11,12). An imbalance between systemic and pulmonary circulation during CPR can also cause lung injury (8,9). Given that early intervention, for example pharmaceutical therapy, or applying protective ventilation and optimal positive end expiratory pressure (PEEP), has been shown to be beneficial for lung injury (13,14), early detection of victims with or at risk of developing acute lung injury after CPR is critical (13).

Despite that blood gas analysis and chest X-rays are commonly used to evaluate lung injury in a clinical setting, those methods do not detect early and quantitatively the severity of lung injury after successful resuscitation from CA (9). Quantitative computed tomography (QCT) can measurably evaluate lung lesions, and is often used for lung function assessment of emphysema, severity of pulmonary fibrosis, edema, and other conditions (15-21). However, to our knowledge, there are no studies of QCT for the assessment of lung injury after successful CPR. In addition, the correlation between downtime and lung injury has not been thoroughly clarified (22).

In the present study, we used QCT to investigate the severity of lung injury after successful CPR in a porcine CA model with different downtimes.

Methods

This is a prospective, randomized and controlled experimental study. Twenty-one male domestic pigs weighing 38±3 kg were randomized into three groups: The sham (n=5), VF5 (n=8), and VF10 (n=8) groups. The animal experiments were approved by the Institutional Animal Care and Use Committee of the Tang Wanchun Laboratories of Emergency & Critical Care Medicine at Sun Yat-sen Memorial Hospital, Sun Yat-sen University (IACUC-SYSU -P1604).

Animal preparation

Animals were fasted overnight, but had free access to water. Anesthesia was initiated by intramuscular injection of ketamine (20 mg/kg), followed by intravascular injection with sodium pentobarbital (30 mg/kg). A cuffed endotracheal tube was introduced into the trachea and a VELA ventilator (CareFushion, California, USA) was used with a tidal volume of 10 mL/kg body weight, peak flow below 40 L/min, and FiO_2 of 0.21. End-tidal carbon dioxide pressure ($ETCO_2$) was measured using the capnometer module of a BeneView T5 patient monitor (Mindray, Shenzhen, China), and respiratory frequency was adjusted to maintain an $ETCO_2$ between 35–45 mmHg. Body temperature was maintained at 37.5±0.5 ℃ throughout the entire experiment. For the collection of blood samples and the measurement of aortic pressure, a 6-F catheter was inserted into the thoracic aorta through the right femoral artery. A 7-F Swan-Ganz^{TM} TD catheter (Edwards Life Sciences LLC, USA) was advanced from the right femoral vein into the right atrium to measure core blood temperature and right atrial pressure. A 5 F pacing catheter (EP Technologies Inc., Mountain View, CA, USA) was placed from the right external jugular vein into the right ventricle. An ECG was monitored during the experiment.

Experimental procedures

Baseline (BL) measurements were obtained fifteen minutes prior to inducing ventricular fibrillation (VF). VF was confirmed by both the ECG waveform and the rapid decrease to 20 mmHg in arterial blood pressure. VF induction and CPR were not performed in the sham group. VF was electrically induced and mechanical ventilation was discontinued after the onset of VF. After untreated VF was

948

Liu et al. Quantitative CT assessment of acute lung injury

maintained for either 5 or 10 minutes for the respective groups, two researchers initiated a two-person manual CPR according to the 2015 AHA guidelines (6). Two minutes after the initiation of CPR, a bolus of epinephrine (20 μg/kg) was administered. Six minutes following CPR, a single 120-J biphasic shock was used to attempt to terminate VF. If an organized rhythm with a mean aortic pressure of >50 mmHg persisted for 5 minutes or more, the animal was regarded as ROSC. If there was a failure of ROSC, CPR was immediately resumed for 2 minutes prior to the attempt of a single second shock. The procedure was repeated for a maximum of 5 cycles. Additional doses of epinephrine were injected at 4-minute intervals after the first injection. If ROSC was not gained, the resuscitation efforts were abandoned.

After resuscitation, all animals were monitored for an additional 6 h. Mechanical ventilation was maintained with 100% inspired oxygen for the first 30 minutes. The oxygen was reduced to 50% for the following 30 minutes, and to 21% thereafter. After 6 h of post-resuscitation care, the animals were transported to perform CT scans.

General measurements

All hemodynamic data were continuously recorded through a data acquisition system supported by Windaq hardware/software (Dataq Instruments Inc., Akron, OH, USA). Arterial blood gas (ABG) was measured at BL and 6 h after resuscitation (ROSC 6 h) with a handheld blood gas analyser (model CG4 + Cartridge, Abbott i-STAT System, Princeton, NJ, USA). Oxygenation index (OI) was calculated as follows, according to ABG analysis: OI = PaO_2/FiO_2.

CT scan protocol and QCT

Chest QCT scans were performed before the animal preparation (BL scan) and 6 hours after ROSC with a 128-slice CT scanner (Siemens Medical Solutions, Germany). The scan protocols were as follows: 120-kVp, 110-mAs, collimation width of 128×0.6 mm, pitch of 0.95, field of view 255 mm × 255 mm, rotation time at 0.5 s/r, slice width of 0.75 mm, no intervals, and reconstructed with B70s kernel. The total time of the QCT image acquisition was approximately 4.9 seconds.

Lung lesion QCT scores were evaluated by two experienced thoracic radiologists according to established methods (23,24). All images were observed with settings optimized for lung evaluation [window width 1,200 Hounsfield units (HU), window level, –600 HU]. Images in 5 levels were evaluated: aortic arch, 1cm above the dome of the right hemidiaphragm, and 3 additional levels equally divided between these two levels. At each level, lungs were segmented into anterior and posterior areas by drawing a horizontal line across the middle of the image, generating four quadrants of analysis per level (23). Lung lesions were quantified in each quadrant per level, including intense parenchymal opacification (IPO) and ground-glass opacification (GGO), with a range of involvement for each sample being assigned a numerical score as follows: 0= normal, 1= <5% involvement, 2= 5–25% involvement, 3= 26–49% involvement, 4= 50–75% involvement, and 5= greater than 75% involvement (23). The scores of the four quadrants were grouped into the total score for each level, and the scores ranged from 0 to 20. The five-level scores were summed to calculate the total lung score (23).

The volume and weight of lung lesions (GGO and IPO) were quantitatively measured on QCT images following previously described methods which classify lung regions according to the degree of aeration as measured by (HU values (15-18) (*Figure 1*). GGO was defined as poorly aerated regions with CT values ranging from –500 to –100 HU, and IPO was defined as non-aerated areas with CT values greater than –100 HU, and those between –900 and –501 HU were normally aerated (15,18). The volume of the GGO and IPO lesions was calculated by volume measurement software (Siemens syngo MultiModality Workstation) based on the range of CT values of the lung lesion. The weight of the lesions was also quantitatively calculated according to the equation previously described {lung tissue weight$_{ROI}$ = total volume$_{ROI}$ × [1 – (mean CT$_{ROI}$/–1000)]} (18,25). Term total volume$_{ROI}$ refers to total lung volume (including normal and abnormal lung tissue), and the mean CT$_{ROI}$ represents the average lung density in HU within each ROI. The lung tissue density was regarded as 1 g/mL in the equation.

Histopathology

All animals were sacrificed after the QCT scan. The removed lungs were rinsed in saline and fixed in a 10% neutral formaldehyde solution. They were then sliced into a 1cm thickness. Specimens were taken from different parts of each lung, including GGO, IPO, and areas without
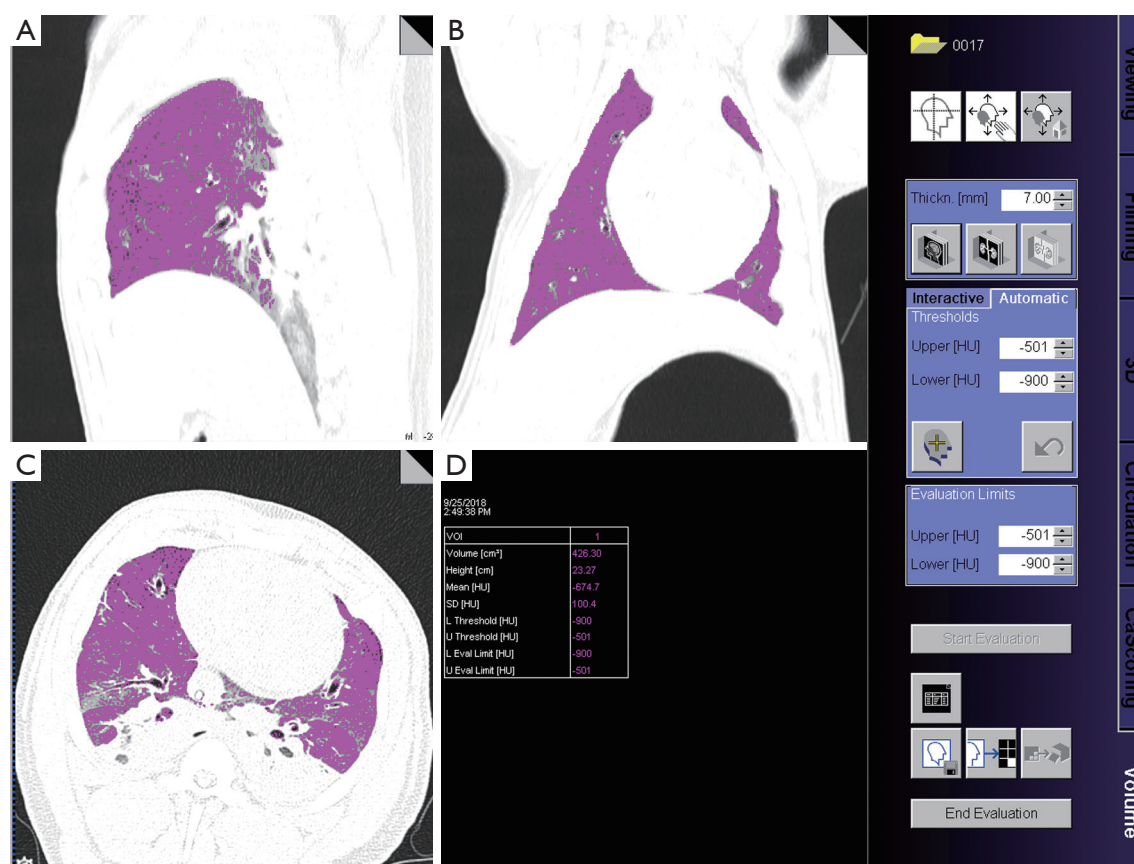
Figure 1 Schematic diagram of lung parenchymal volume measurement. (A-C) The lung parenchyma with a CT value of –501 to –900 HU is shown in the coronal, axial, and sagittal images with pink colour. (D) The automatic measurement results showed that the lung tissue volume with a CT value of –501 to –900 HU was 426.30 cm^3, which is normal lung volume. The lung tissue volume of other ranges of CT values was also measured according to the method described in the manuscript. CT, computed tomography; HU, Hounsfield unit.

obvious lesions. The specimens were embedded in paraffin, and sections 4.5 μm thick were prepared and stained with hematoxylin and eosin for pathological observation.

Statistical analysis

All data were analyzed with SPSS 13.0 for Windows (SPSS, Chicago, IL, USA). Continuous variables were presented as mean ± SD if data were normally distributed, and categorical variables as count and percentage. Continuous variables were compared (pair-wise) between the three study groups with Student's *t*-test. Changes between the baseline and after resuscitation were compared using Student's paired *t*-test. ANOVA with Scheffe's adjustment for multiple comparisons was used among the three groups (the sham, VF5, and VF10 groups). For the comparison of categorical variables, Fisher's exact test was used. A P value of <0.05 was regarded as statistically significant.

Results

Baseline physiology, CPR outcome, and ABG

Eight animals in the VF5 (8/8, 100%) group and six (6/8, 75%) in the VF10 group were successfully resuscitated. Two animals (2/8, 25%) in VF10 group failed to resuscitate. There were no significant differences in the baseline physiological conditions among the three groups (*Table 1*). No obvious differences in PH value, PO$_2$, or OI were observed among these groups at baseline or 6 hours after resuscitation (*Table 1*). Compared with the VF10 group, a significantly shorter duration of resuscitation, fewer defibrillations, and fewer epinephrine doses were observed

950

Liu et al. Quantitative CT assessment of acute lung injury

Table 1 Baseline physiological information and gas exchanges

Variable	VF5, n=8	VF10, n=6	Sham, n=5
Weight, kg	37.9±3.8	38.5±2.4	39.3±4.1
Core temperature, ℃	37.5±0.6	37.8±0.8	37.3±0.4
Heart rate, beats/min	127±20	131±17	117±22
MAP, mmHg	134±27	139±22	124±29
RAP, mmHg	4.9±1.9	5.4±2.2	4.2±1.5
End-tidal CO_2, mmHg	38±3	41±2	36±6
PH at baseline	7.47±0.05	7.45±0.05	7.49±0.09
PH at ROSC 6 h	7.51±0.07	7.54±0.08	7.52±0.11
PO_2 at baseline, mmHg	79±7	76±10	83±11
PO_2 at ROSC 6 h, mmHg	75±9	71±13	78±12
OI at baseline, mmHg	376±33	362±48	395±52
OI at ROSC 6 h, mmHg	357±43	338±62	371±57

Values are presented as mean ± SD. MAP, mean artery pressure; RAP, right atrium pressure, ROSC 6 h, 6 hours post-resuscitation, OI, oxygen index.

Table 2 Outcomes of CPR

Variable	VF5, n=8	VF10, n=6	P value
Duration of CPR, minutes	6±0	8.3±1.5	<0.05
Numbers of defibrillation, n	1±0	2.2±0.8	<0.05
Total dosage of EPI, n	1±0	1.8±0.4	<0.05

Values are presented as mean ± SD. CPR, cardiopulmonary resuscitation; EPI, epinephrine.

in the VF5 group (*Table 2*).

QCT findings

The baseline QCT scans of all animal models showed that their lungs and skeletal thoraxes were normal. However, chest QCTs showed that all animals in both the VF5 and VF10 groups were found to have GGO and IPO at ROSC 6 h (*Figure 1*). The GGO was diffusely distributed in the bilateral lungs (most prominent in the lower lobe), which displayed uneven density with blurred edges, and did not show characteristic "wing-like" distributions of cardiogenic pulmonary edema. The bronchial and pulmonary vascular markings were seen in the GGO area on QCT images (*Figure 1*). The IPO was mainly distributed in the lower dorsal region of bilateral lungs, which were well defined with uniform density. The pulmonary vascular markings did not show in the IPO area on QCT images (*Figure 2*).

In addition, rib fractures were observed in both VF groups, which were more common in the bilateral third-sixth anterior ribs, and two cases of hydrothorax in the VF5 group and two cases of hydropericardium in the VF10 group were detected (*Tables 3* and *4*).

QCT measurement

The GGO QCT score, volume, and weight were significantly higher in the VF10 than those in the VF5 group at ROSC 6h (P=0.002, 0.001, and 0.002 respectively). No significant differences were found between the two VF groups for IPO QCT score, volume, or weight after resuscitation (P=0.354, 0.447, and 0.512 respectively) (*Figure 2*).

Histopathology

The hemorrhage and consolidation area was observed in the lungs of the VF groups on gross pathological examination. Microscopically, histopathological changes of lung injury were observed in both VF groups. Pathological changes such as neutrophils and erythrocytes in the alveolar space and alveolar walls, exudate and fibrin-like fillers in the alveolar space, and formation of hyaline membranes were noted in the GGO areas. The IPO areas showed collapse or disappearance of alveoli, a significant widening of the alveolar septum, and the obvious presence of red blood cells in the alveolar cavity and interstitial spaces pathologically. There were no histopathological changes in the sham group (*Figure 3*).

Discussion

In the present study, QCT was first utilized to promptly and quantitatively detect lung injury, and then to evaluate its severity after successful resuscitation in a porcine CA model with different downtimes (5 and 10 mins). All the animals in both VF groups were found to have GGO and IPO in QCT images after resuscitation. Moreover, the QCT score, volume, and weight of GGO were significantly higher in the VF10 group than the VF 5 group while there were no differences in IPO between the two VF groups. Histopathological results provided further evidence for the QCT findings.

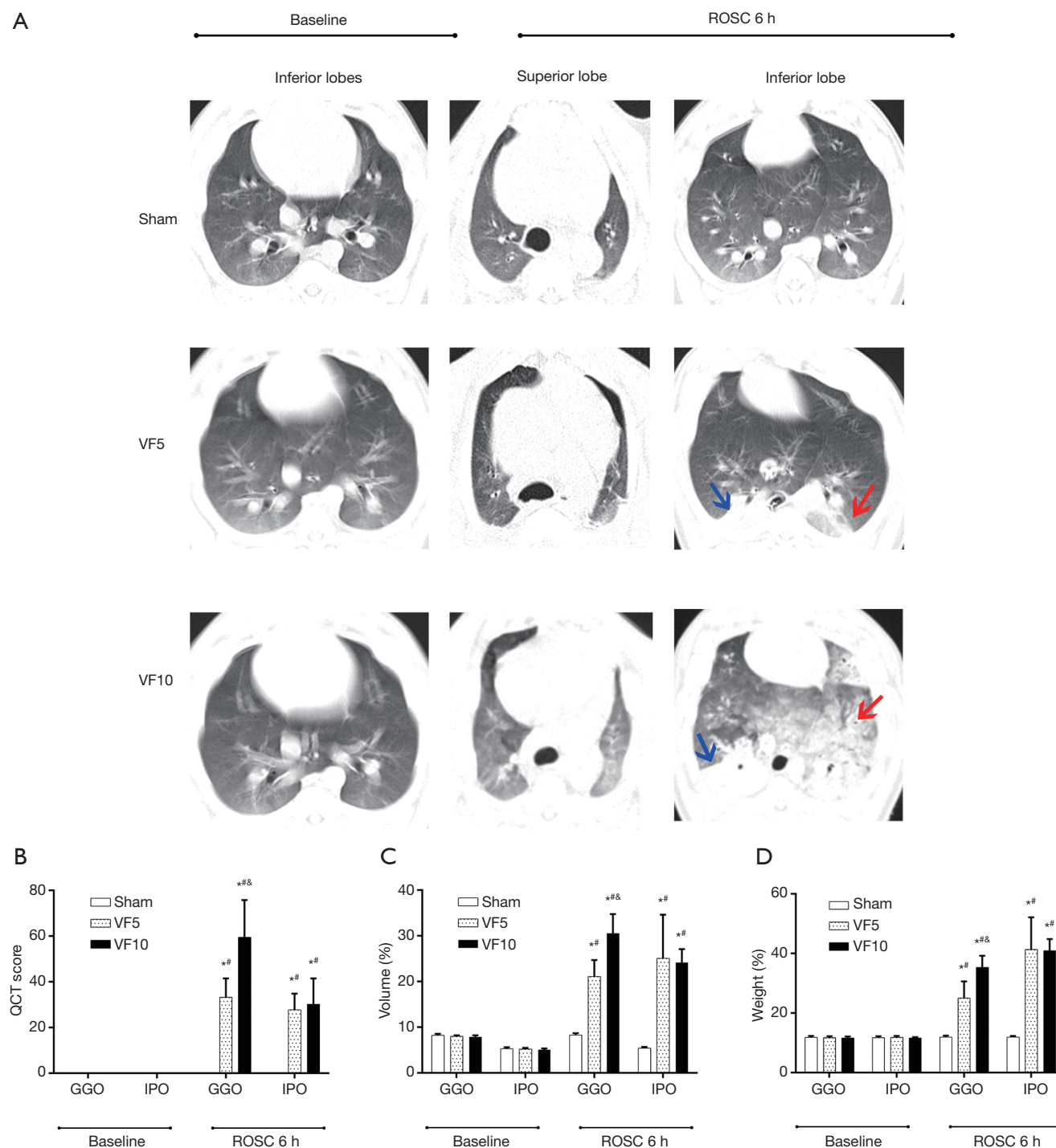The Berlin definition for acute injury and acute respiratory disease syndrome (ARDS) was OI ≤300 mmHg (26).

Figure 2 Lung injury on the QCT before and 6 h after cardiac arrest and resuscitation. (A) Axial CT images showed that GGO (red arrow) and IPO (blue arrow) were found in the VF5 and VF10 groups at 6 h after successful resuscitation. The QCT scores (B), volume (C), and weight (D) of GGO in VF5 were significantly higher than in VF10 6 hours after successful resuscitation, and neither of these IPO values in VF5 had significant differences with VF10 at 6 hours after successful resuscitation. *: *vs.* baseline; #: *vs.* sham group; &: *vs.* VF5 group. P<0.05. QCT, quantitative computed tomography; GGO, ground-glass opacification; IPO, intense parenchymal opacification; VF, ventricular fibrillation.

952

Liu et al. Quantitative CT assessment of acute lung injury

Table 3 Comparison of the rate of complication after CPR between VF5 and VF10 group

Injury	VF5, n=8	VF10, n=6
Rib fracture rate	5 (62.5%)	4 (66.7%)
No. of rib fracture		
Single	0	0
Multiple	5 (100%)	4 (100%)
Side of rib fracture		
Right	0	0
Left	3 (60%)	2 (50%)
Both	2 (40%)	2 (50%)
Site of rib fracture		
Anterior	5 (100%)	4 (100%)
Posterior	0	0
Axilla	0	0
Pneumothorax	1 (12.5%)	1 (16.7%)
Hydrothorax	2 (25%)	0
Hydropericardium	0	2 (33.3%)

VF, ventricular fibrillation; n, number of cases.

Table 4 Rib fracture

Rib No.	VF 5 min		VF 10 min	
	Right (n)	Left (n)	Right (n)	Left (n)
1	0	0	0	0
2	0	0	0	0
3	0	4	0	4
4	2	5	3	4
5	2	4	0	4
6	0	2	2	4
7	0	2	0	0
8	0	0	0	0
9	0	0	0	0
10	0	0	0	0
11	0	0	0	0
12	0	0	0	0
13	0	0	0	0
14	0	0	0	0

VF, ventricular fibrillation; n, number of case.

Acute lung injury (ALI)/ARDS is a rapidly progressive pathophysiological process, and often is the main reason for ICU admission (13). In the present study, we found that there were no significant differences in OI among the three groups (Sham, VF5, and VF10 groups) at 6 h after resuscitation, but obvious GGO and IPO changes on bilateral lungs were detected by QCT in both VF groups at 6 h after ROSC, which were histopathologically confirmed. Therefore, we speculate that QCT is a more sensitive method for the early detection of lung injury than OI.

Lung injury is detected as GGO and IPO on a QCT scan. GGO is considered to be a manifestation of pulmonary edema, which is usually found in pulmonary tissues of hemodynamic dysfunction, toxic injury, or embolism (27,28). Pulmonary edema is a very common pathological characteristic of lung injury following CPR, and severe pulmonary edema is a major cause of failing lung function, which is correlated with a poor long-term prognosis (29,30). In our study, GGO was found in the QCT images in all animals of both VF groups at 6 hours after ROSC, and histopathological results confirmed that the GGO area in QCT scans was pulmonary edema. The

GGO lesions were diffusely distributed with blurred edges, and did not show characteristic "wing-like" distribution of cardiogenic pulmonary edema. Cho *et al.* also found similar results in 44 patients who underwent CT scans after CPR (9). Additionally, in a study by Wang *et al.* (30) where twenty-eight pigs were randomized into three groups, it was found that extra-vascular lung fluid significantly increased in a continuous compression group compared to a 30:2 compression/rescue ventilation CPR group (30). This suggests that a long-term CPR can aggravate pulmonary edema. We also found that the animals in our VF5 group required a significantly shorter duration of CPR, and the GGO QCT score, volume, and weight in the VF10 group was significantly higher than in the VF5 group. These results illustrate the more serious pulmonary edema in the VF10 group. A longer duration of CA downtime means a lower success rate of resuscitation and a longer time of organ ischemia, which brings about a more serious lung injury after resuscitation (31). Therefore, the presence of pulmonary edema may be associated with CA downtime.

IPO was a reflection of physical injuries after CPR and defined as an obvious increase in lung opacity on the QCT images, which was pathologically confirmed as the
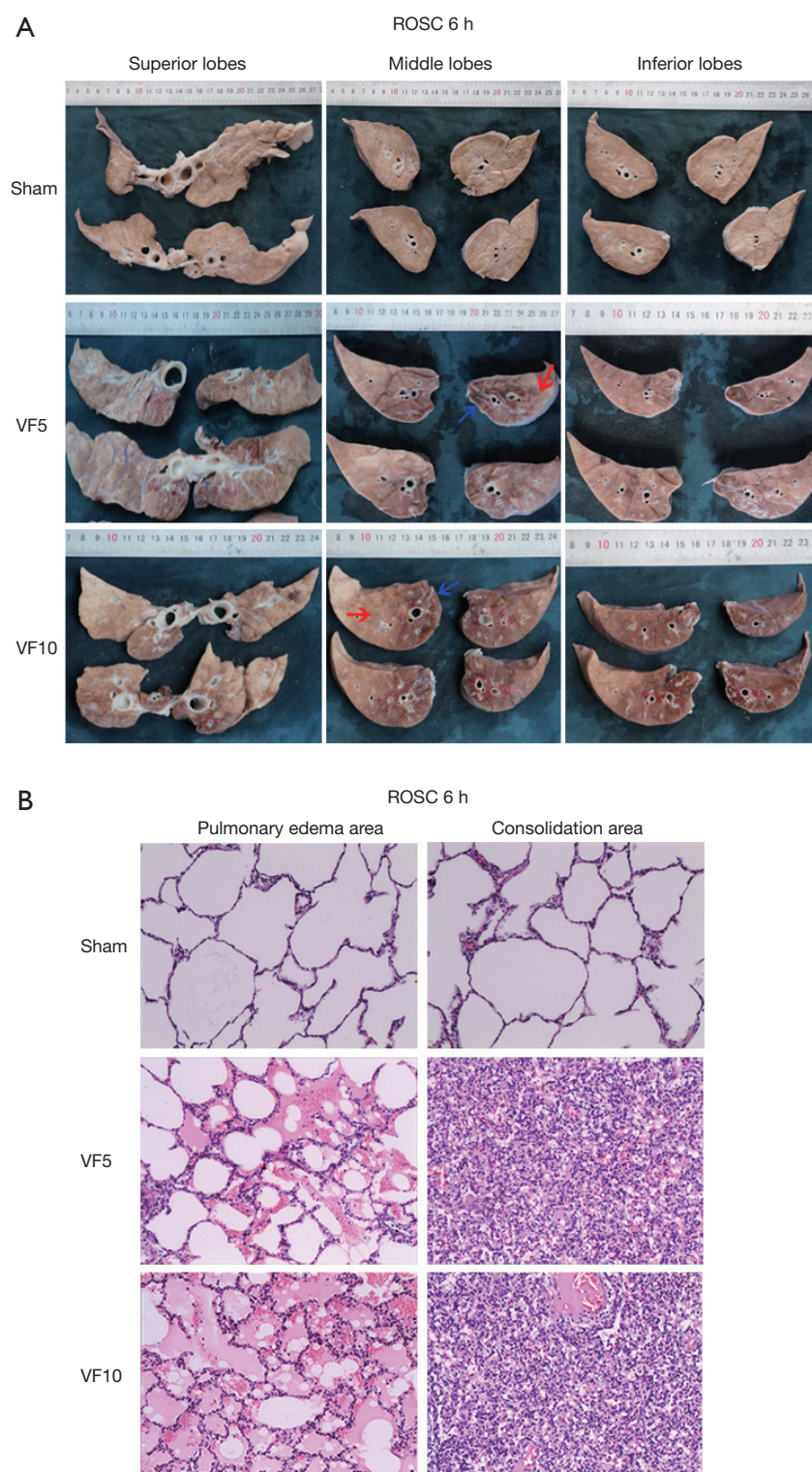
Figure 3 Histopathological changes for lung injury after cardiac arrest and resuscitation. (A) Gross pathological specimens were shown that edema (red arrow) and atelectasis (blue arrow) in the VF groups at 6 hours after ROSC. (B) Routine hematoxylin-eosin (HE ×100) staining procedure shows that exudate including red blood cells and inflammatory cells were present in the alveolar cavity of the pulmonary edema area in VF groups. ROSC, restoration of spontaneous circulation; VF, ventricular fibrillation.

collapse or disappearance of alveoli, a significant widening of the alveolar septum, and the obvious presence of red blood cells in the alveolar cavity and interstitial spaces (30). IPO was found on the QCT images in all animals of both VF groups after ROSC, and the IPO area in QCT was pathologically proven in our study to be pulmonary atelectasis and pneumorrhagia. QCT score, volume, and weight of IPO were not significantly different between the VF5 and VF10 groups. This implies that the presence of IPO was not associated with the downtime of CA. The mechanism of pulmonary IPO after CPR has not yet been defined; however, chest compression is a risk factor for IPO. Beom *et al.* suggested that an increased length of CPR administration is a risk factor for the development of pneumorrhagia (32). Markstaller *et al.* used dynamic CT to assess the effects of chest compression during CPR on alveolar recruitment and hemodynamic parameters in a porcine VF model (33). They found that cyclic collapse and recruitment of lung parenchyma likely caused a variation in the shunt fraction over time and the impairment of gas exchange, which subsequently led to atelectasis.

Early quantitative assessment of lung injury contributes to ventilation strategy management, and can reduce ventilator-induced lung injury risks (34). Klapsing *et al.* used QCT to quantitatively measure the volume of lung lesions in 10 mechanically ventilated patients with mild to moderate ARDS. They found that QCT can identify patients with high rates of lung overdistension under high airway pressure, and may help initiate early lung protection strategies to reduce airway pressure and reduce the risk of lung injury from ventilators (34). Chen *et al.* used QCT to assess an oleic acid-induced canine ARDS model, and found that QCT parameters, particular percentages of non-aerated lung areas, as well as mean CT attenuation values and tissue mass, can detect ARDS with high sensitivity and specificity at an early stage. This provides assistance for the early diagnosis of ARDS (35), which may be of clinical relevance in a mechanical ventilation setting.

Rib fractures were observed in both VF5 and VF10 groups, and the results are similar to those of Kim *et al.* (36). Other thoracic injuries such as pneumothorax, hydrothorax, and hydropericardium observed in VF groups should also be noted, since these thoracic injuries may also affect resuscitation outcomes.

There were several limitations to the present study. First, a healthy porcine model does not always indicate the real conditions of human patients in a clinical setting. Second, our QCT scans only reflected the changes at 6 hours after ROSC, without dynamic observation of the progression of lung injury. Third, this is a small sample size study and that may have an effect on some results.

Conclusions

Lung injury is a common complication after resuscitation, and more severe lung injury results from prolonged CA. QCT analysis enables unique non-invasive assessments of different acute lung injuries (IPO and GGO lesions) that can clearly distinguish heterogeneous lesions and allow for early detection and quantitative monitoring of the severity of lung injury following CPR. QCT may provide a basis for clinical early ventilation strategy management after CPR.

Acknowledgements

Footnote

Conflicts of Interest: The authors have no conflicts of interest to declare.

Ethical Statement: The study was approved by the Institutional Animal Care and Use Committee of the Tang Wanchun Laboratories of Emergency & Critical Care Medicine at Sun Yat-sen Memorial Hospital, Sun Yat-sen University (IACUC-SYSU-P1604).

References

1. Angus DC. Successful Resuscitation From In-Hospital Cardiac Arrest--What Happens Next? JAMA 2015;314:1238-9.
2. Sasson C, Rogers MA, Dahl J, Kellermann AL. Predictors of survival from out-of-hospital cardiac arrest: a systematic review and meta-analysis. Circ Cardiovasc Qual Outcomes 2010;3:63-81.
3. Buschmann CT, Tsokos M. Frequent and rare complications of resuscitation attempts. Intensive Care Med 2009;35:397-404.
4. Miller AC, Rosati SF, Suffredini AF, Schrump DS. A systematic review and pooled analysis of CPR-associated

cardiovascular and thoracic injuries. Resuscitation 2014;85:724-31.

5. Berg RA, Hemphill R, Abella BS, Aufderheide TP, Cave DM, Hazinski MF, Lerner EB, Rea TD, Sayre MR, Swor RA. Part 5: adult basic life support: 2010 American Heart Association Guidelines for Cardiopulmonary Resuscitation and Emergency Cardiovascular Care. Circulation 2010;122:S685-705.

6. Kleinman ME, Brennan EE, Goldberger ZD, Swor RA, Terry M, Bobrow BJ, Gazmuri RJ, Travers AH, Rea T. Part 5: Adult Basic Life Support and Cardiopulmonary Resuscitation Quality: 2015 American Heart Association Guidelines Update for Cardiopulmonary Resuscitation and Emergency Cardiovascular Care. Circulation 2015;132:S414-35.

7. Ihnát Rudinská L, Hejna P, Ihnát P, Tomášková H, Smatanová M, Dvořáček I. Intra-thoracic injuries associated with cardiopulmonary resuscitation - Frequent and serious. Resuscitation 2016;103:66-70.

8. Cha KC, Kim YW, Kim HI, Kim OH, Cha YS, Kim H, Lee KH, Hwang SO. Parenchymal lung injuries related to standard cardiopulmonary resuscitation. Am J Emerg Med 2017;35:117-21.

9. Cho SH, Kim EY, Choi SJ, Kim YK, Sung YM, Choi HY, Cho J, Yang HJ. Multidetector CT and radiographic findings of lung injuries secondary to cardiopulmonary resuscitation. Injury 2013;44:1204-7.

10. Slutsky AS, Ranieri VM. Ventilator-induced lung injury. N Engl J Med 2013;369:2126-36.

11. Al-Mehdi AB, Shuman H, Fisher AB. Intracellular generation of reactive oxygen species during nonhypoxic lung ischemia. Am J Physiol 1997;272:L294-300.

12. Nolan JP, Neumar RW, Adrie C, Aibiki M, Berg RA, Bottiger BW, Callaway C, Clark RS, Geocadin RG, Jauch EC, Kern KB, Laurent I, Longstreth WT, Merchant RM, Morley P, Morrison LJ, Nadkarni V, Peberdy MA, Rivers EP, Rodriguez-Nunez A, Sellke FW, Spaulding C, Sunde K, Hoek TV. Post-cardiac arrest syndrome: epidemiology, pathophysiology, treatment, and prognostication. A Scientific Statement from the International Liaison Committee on Resuscitation; the American Heart Association Emergency Cardiovascular Care Committee; the Council on Cardiovascular Surgery and Anesthesia; the Council on Cardiopulmonary, Perioperative, and Critical Care; the Council on Clinical Cardiology; the Council on Stroke. Resuscitation 2008;79:350-79.

13. Chbat NW, Chu W, Ghosh M, Li G, Li M, Chiofolo CM, Vairavan S, Herasevich V, Gajic O. Clinical knowledge-based inference model for early detection of acute lung injury. Ann Biomed Eng 2012;40:1131-41.

14. Briel M, Meade M, Mercat A, Brower RG, Talmor D, Walter SD, Slutsky AS, Pullenayegum E, Zhou Q, Cook D, Brochard L, Richard JC, Lamontagne F, Bhatnagar N, Stewart TE, Guyatt G. Higher vs lower positive end-expiratory pressure in patients with acute lung injury and acute respiratory distress syndrome: systematic review and meta-analysis. JAMA 2010;303:865-73.

15. Derosa S, Borges JB, Segelsjo M, Tannoia A, Pellegrini M, Larsson A, Perchiazzi G, Hedenstierna G. Reabsorption atelectasis in a porcine model of ARDS: regional and temporal effects of airway closure, oxygen, and distending pressure. J Appl Physiol (1985) 2013;115:1464-73.

16. Knoll MA, Salvatore M, Sheu RD, Knoll AD, Kerns SL, Lo YC, Rosenzweig KE. The use of isodose levels to interpret radiation induced lung injury: a quantitative analysis of computed tomography changes. Quant Imaging Med Surg 2016;6:35-41.

17. Ruth Graham M, Goertzen AL, Girling LG, Friedman T, Pauls RJ, Dickson T, Espenell AE, Mutch WA. Quantitative computed tomography in porcine lung injury with variable versus conventional ventilation: recruitment and surfactant replacement. Crit Care Med 2011;39:1721-30.

18. Xin Y, Song G, Cereda M, Kadlecek S, Hamedani H, Jiang Y, Rajaei J, Clapp J, Profka H, Meeder N, Wu J, Tustison NJ, Gee JC, Rizi RR. Semiautomatic segmentation of longitudinal computed tomography images in a rat model of lung injury by surfactant depletion. J Appl Physiol (1985) 2015;118:377-85.

19. Gierada DS, Guniganti P, Newman BJ, Dransfield MT, Kvale PA, Lynch DA, Pilgram TK. Quantitative CT assessment of emphysema and airways in relation to lung cancer risk. Radiology 2011;261:950.

20. Ley B, Elicker BM, Hartman TE, Ryerson CJ, Vittinghoff E, Ryu JH, Lee JS, Jones KD, Richeldi L, Jr TEK. Idiopathic Pulmonary Fibrosis: CT and Risk of Death. Radiology 2014;273:570-9.

21. Çetinçakmak MG, Göya C, Hamidi C, Tekbaş G, Abakay Ö, Batmaz İ, Hattapoğlu S, Yavuz A, Bilici A. Quantitative volumetric assessment of pulmonary involvement in patients with systemic sclerosis. Quant Imaging Med Surg 2016;6:50-6.

22. Markstaller K, Karmrodt J, Doebrich M, Wolcke B, Gervais H, Weiler N, Thelen M, Dick W, Kauczor HU, Eberle B. Dynamic computed tomography: a novel technique to study lung aeration and atelectasis formation during experimental CPR. Resuscitation 2002;53:307-13.

23. Burnham EL, Hyzy RC, Paine R 3rd, Coley C 2nd, Kelly AM, Quint LE, Lynch D, Janssen WJ, Moss M, Standiford TJ. Chest CT features are associated with poorer quality of life in acute lung injury survivors. Crit Care Med 2013;41:445-56.

24. Ichikado K, Suga M, Muranaka H, Gushima Y, Miyakawa H, Tsubamoto M, Johkoh T, Hirata N, Yoshinaga T, Kinoshita Y, Yamashita Y, Sasaki Y. Prediction of prognosis for acute respiratory distress syndrome with thin-section CT: validation in 44 cases. Radiology 2006;238:321-9.

25. Gattinoni L, Caironi P, Pelosi P, Goodman LR. What has computed tomography taught us about the acute respiratory distress syndrome? Am J Respir Crit Care Med 2001;164:1701-11.

26. ARDS Definition Task Force, Ranieri VM, Rubenfeld GD, Thompson BT, Ferguson ND, Caldwell E, Fan E, Camporota L, Slutsky AS. Acute respiratory distress syndrome: the Berlin Definition. JAMA 2012;307:2526-33.

27. Scillia P, Delcroix M, Lejeune P, Melot C, Struyven J, Naeije R, Gevenois PA. Hydrostatic pulmonary edema: evaluation with thin-section CT in dogs. Radiology 1999;211:161-8.

28. Thoma P, Rondelet B, Melot C, Tack D, Naeije R, Gevenois PA. Acute pulmonary embolism: relationships between ground-glass opacification at thin-section CT and hemodynamics in pigs. Radiology 2009;250:721-9.

29. Kang DH, Kim J, Rhee JE, Kim T, Kim K, Jo YH, Lee JH, Lee JH, Kim YJ, Hwang SS. The risk factors and prognostic implication of acute pulmonary edema in resuscitated cardiac arrest patients. Clin Exp Emerg Med 2015;2:110-6.

30. Wang S, Wu JY, Guo ZJ, Li CS. Effect of rescue breathing during cardiopulmonary resuscitation on lung function after restoration of spontaneous circulation in a porcine model of prolonged cardiac arrest. Crit Care Med 2013;41:102-10.

31. Weisfeldt ML, Becker LB. Resuscitation after cardiac arrest: a 3-phase time-sensitive model. JAMA 2002;288:3035-8.

32. Beom JH, You JS, Kim MJ, Seung MK, Park YS, Chung HS, Chung SP, Park I. Investigation of complications secondary to chest compressions before and after the 2010 cardiopulmonary resuscitation guideline changes by using multi-detector computed tomography: a retrospective study. Scand J Trauma Resusc Emerg Med 2017;25:8.

33. Markstaller K, Rudolph A, Karmrodt J, Gervais HW, Goetz R, Becher A, David M, Kempski OS, Kauczor HU, Dick WF, Eberle B. Effect of chest compressions only during experimental basic life support on alveolar collapse and recruitment. Resuscitation 2008;79:125-32.

34. Klapsing P, Herrmann P, Quintel M, Moerer O. Automatic quantitative computed tomography segmentation and analysis of aerated lung volumes in acute respiratory distress syndrome-A comparative diagnostic study. J Crit Care 2017;42:184-91.

35. Chen H, Zeng QS, Chen RC, Li W, Zhou JX, Liu Q, Dai WC. Early quantitative CT analysis of oleic acid induced acute respiratory distress syndrome in a canine model. Int J Clin Exp Med 2015;8:7015-28.

36. Kim EY, Yang HJ, Sung YM, Cho SH, Kim JH, Kim HS, Choi HY. Multidetector CT findings of skeletal chest injuries secondary to cardiopulmonary resuscitation. Resuscitation 2011;82:1285-8.